Feasibility of poly(ethylene glycol) derivatives as diagnostic drug carriers for tumor imaging

Kengo Kanazaki, Kohei Sano, Akira Makino, Fumio Yamauchi, Atsushi Takahashi, Tsutomu Homma, Masahiro Ono, Hideo Saji

PII: S0168-3659(16)30070-0
DOI: doi: 10.1016/j.jconrel.2016.02.017
Reference: COREL 8130

To appear in: *Journal of Controlled Release*

Received date: 27 October 2015
Revised date: 26 January 2016
Accepted date: 6 February 2016

Please cite this article as: Kengo Kanazaki, Kohei Sano, Akira Makino, Fumio Yamauchi, Atsushi Takahashi, Tsutomu Homma, Masahiro Ono, Hideo Saji, Feasibility of poly(ethylene glycol) derivatives as diagnostic drug carriers for tumor imaging, *Journal of Controlled Release* (2016), doi: 10.1016/j.jconrel.2016.02.017

Journal of Controlled Release

Title

Feasibility of poly(ethylene glycol) derivatives as diagnostic drug carriers for tumor imaging

The names, affiliations, and addresses of the authors

Kengo Kanazaki[a,b], Kohei Sano[a,c], Akira Makino[a,d], Fumio Yamauchi[b], Atsushi Takahashi[b], Tsutomu Homma[b], Masahiro Ono[a], Hideo Saji[a,*]

[a]*Department of Patho-Functional Bioanalysis Graduate School of Pharmaceutical Sciences, Kyoto University, 46-29 Yoshida Shimoadachi-cho, Sakyo-ku, Kyoto, Japan, 606-8501*

[b]*Medical Imaging Project, Corporate R&D Headquarters, Canon Inc., 3-30-2 Shimomaruko, Ohta-ku, Tokyo, Japan, 146-8501*

[c]*Kyoto University Hospital, 54 Kawaharacho, Shogoin, Sakyo-ku, Kyoto, Japan, 606-8507*

[d]*Biomedical Imaging Research Center, University of Fukui, 23-3 Matsuokashimoaizuki, Eiheiji-cho, Yoshida-gun, Fukui, Japan, 910-1193*

*** Corresponding author**

Hideo Saji, PhD, Professor

Department of Patho-Functional Bioanalysis Graduate School of Pharmaceutical Sciences, Kyoto University; 46-29 Yoshida Shimoadachimachi, Sakyo-ku, Kyoto 606-8501, Japan

Tel: +81-75-753-4556 Fax: +81-75-753-4568

E-mail: hsaji@pharm.kyoto-u.ac.jp

ABSTRACT (218 words)

Poly(ethylene glycol) (PEG) is an artificial but biocompatible hydrophilic polymer that has been widely used in clinical products. To evaluate the feasibility of using PEG derivative itself as a tumor imaging carrier *via* an enhanced permeability and retention (EPR) effect, we prepared indium-111-labeled PEG (^{111}In-DTPA-PEG) and indocyanine green (ICG)-labeled PEG (ICG-PEG) with PEG molecular weights of 5–40 kDa and investigated their *in vivo* biodistribution in colon26 tumor-bearing mice. Thereafter, single-photon emission computed tomography (SPECT) and photoacoustic (PA) imaging studies were performed. The i*n vivo* biodistribution studies demonstrated increased tumor uptake and a prolongation of circulation half-life as the molecular weight of PEG increased. Although the observed differences in *in vivo* biodistribution were dependent on the labeling method (^{111}In or ICG), the tumor-to-normal tissue ratios were comparable. Because PEG-based probes with a molecular weight of 20 kDa (PEG20) showed a preferable biodistribution (highest accumulation among tissues excised and relatively high tumor-to-blood ratios), an imaging study using ^{111}In-DTPA-PEG20 and ICG-PEG20 was performed. Colon26 tumors inoculated in the right shoulder or flank were clearly visualized by SPECT 24 h after administration. Furthermore, PA imaging using ICG-PEG20 also detected tumor regions, and the detected PA signals increased in proportion with the injected dose. These results suggest that PEG derivatives (20 kDa) serve as robust diagnostic drug carriers for tumor imaging.

Keywords:

Cancer diagnosis, poly(ethylene glycol), indocyanine green, photoacoustic imaging, single-photon emission computed tomography

1. Introduction

Nanosized delivery vehicles, including liposomes, nanomicelles, and nanoparticles, have a potential utility as diagnostic and therapeutic drug carriers targeting tumors because of their capacity to deliver a large drug payload [1,2]. In general, nanomaterials are rapidly endocytosed by the reticuloendothelial cells in the liver and spleen when administered intravenously [3], which could shorten the duration of *in vivo* circulation. This uptake decreases tumor uptake *via* the enhanced permeability and retention (EPR) effects by which macromolecules can preferentially accumulate within the tumor tissues [4,5]. To improve the *in vivo* pharmacokinetics and assure nanomaterial *in vivo* stability, most nanomaterials are coated with poly(ethylene glycol) (PEG) on their surface to increase particle hydrophilicity [6,7]. In addition, several bioactive proteins conjugated with biocompatible PEG have been widely used in clinical products [8,9] to optimize their *in vivo* biodistribution.

PEG characteristics include the following: 1) high solubility in aqueous solutions; 2) low toxicity and high biocompatibility [9]; 3) facile PEG modification through the terminal attachment of various types of functional groups; and 4) availability of a wide range of molecular weights [10]. Although high molecular weight PEG molecule itself could be speculated to exhibit increased tumor uptake *via* the EPR effect, there has been no report on this research. Therefore, we proposed that PEG derivatives (PEG chain possessing functional group at termini) can be novel diagnostic drug carriers for tumor imaging based on the EPR effect, and clarified favorable molecular weight of PEG for *in vivo* tumor imaging *via* EPR effect. In this study, we focused on two distinct imaging modalities: single-photon emission computed tomography (SPECT) and photoacoustic (PA) imaging. SPECT is a nuclear medical imaging technique widely used in clinical that enables the performance of a whole body scan. PA imaging is a form of optical imaging that has a potential for intraoperative diagnosis [11,12]. PA imaging noninvasively detects ultrasonic waves thermoelastically induced by optical absorbers (i.e., a fluorescent dye and metal nanoparticles) irradiated with a pulsed laser [13]. The ultrasonic waves display much lower tissue scattering, leading to penetration depths of multiple centimeters and sub-millimeter spatial resolution [14]. Thus, PA imaging has the potential for a broader clinical application than other forms of optical imaging, and the development of contrast agents for PA tumor imaging has been strongly desired. For SPECT and PA imaging, we prepared PEG molecules labeled with a radioisotope [indium-111: ^{111}In, $t_{1/2}$ = 2.8 days; γ-radiation, 171 keV (90%), 254 keV (94%)] using diethylene triamine pentaacetic acid (DTPA) as a metal chelator and PEG conjugated with a fluorescent dye (indocyanine green; ICG), respectively. ICG is a US Food and Drug Administration (FDA)-approved material that has been applied to the assessment of liver function and retinal angiography [15,16]. Because of absorptions in the near-infrared window [17], ICG is suitable for *in vivo* PA imaging [18-20].

Herein, this study first assessed the quantitative *in vivo* biodistribution of ^{111}In-DTPA-PEG and ICG-PEG in tumor-bearing mice because there was a possibility that pharmacokinetics of PEG derivatives could be altered relative to the physicochemical properties of the molecules (signal emitters) conjugated to PEG. Subsequently, we evaluated the feasibility of using PEG derivatives as tumor diagnostic drug carriers through an *in vivo* imaging study incorporating SPECT and PA imaging.

2. Material and methods

2.1 Materials

α-Aminoethyl-ω-methoxy poly(oxyethylene) (monoamino PEG, SUNBRIGHT ME-EA series, molecular weight: 5, 10, 20, and 40 kDa) and α-aminopropyl-ω-aminopropyl poly(oxyethylene) (diamino PEG, SUNBRIGHT DE-PA series, molecular weight: 20 kDa)

were purchased from NOF Co. (Tokyo, Japan). Each monoamino PEG is hereinafter referred to as PEG5, PEG10, PEG20, and PEG40 according to the molecular weight of each PEG formulation. Hydrodynamic diameter of each monoamino PEG was measured by dynamic light scattering (DLS) with the Zetasizer nano (Malvern Instruments Ltd. (Worcestershire, UK.)). S-2-(4-Isothiocyanatobenzyl)-diethylene triamine pentaacetic acid (p-SCN-Bn-DTPA) was purchased from Macrocyclics Inc. (Dallas, TX, USA). N,N-Diisopropylethylamine (DIPEA), potassium iodide, and iodine were purchased from Nacalai tesque, Inc. (Kyoto, Japan). Barium chloride was purchased from Wako Pure Chemical Industries, Ltd. (Osaka, Japan). ICG was purchased from the Pharmaceutical and Medical Device Regulatory Science Society of Japan (Tokyo, Japan). 2-[7-[1,3-Dihydro-1,1-dimethyl-3-(4-sulfobutyl)-2H-benzo[e]indol-2-ylidene]-1,3,5-heptatrienyl]-1,1-dimethyl-3-[5-(3-sulfosuccinimidyl)oxycarbonylpentyl]-1H-benzo[e]indolium, inner salt, sodium salt (ICG-Sulfo-OSu) was purchased from Dojindo Molecular Technologies, Inc. (Kumamoto, Japan). ^{111}In chloride ($^{111}InCl_3$) (74 MBq/mL in 0.02 N HCl) was purchased from Nihon Medi-Physics (Tokyo, Japan). All other chemicals used were of the highest purity available.

2.2 Preparation of PEG conjugates

2.2.1 DTPA-PEG

For radiolabeling with ^{111}In, a DTPA derivative cationic metal chelator was introduced to PEG. Each monoamino PEG (1.0 μmol in 1 mL chloroform) was mixed with *p*-SCN-Bn-DTPA [2.0 μmol in 1 mL *N*,*N*-dimethylformamide (DMF)] and DIPEA (2.0 μmol in 10 μL chloroform) at a molar ratio of PEG:DTPA = 1:2 and was incubated at room temperature (r.t.) for 24 h. After solvent evaporation, the resulting mixture was dissolved in Tris-HCl buffer (20 mM, pH 9.0) and purified by ultrafiltration with Amicon Ultra centrifugal filter units [molecular weight cut-off (MWCO): 3 kDa for PEG5 and PEG10 and 10 kDa for PEG20 and PEG40] (Merck Millipore, Co., Billerica, MA, USA) to remove unconjugated DTPA. After three times of ultrafiltration, the resulting solution was purified on an anion exchange chromatography system (AKTApurifier 10, GE Healthcare, Little Chalfont, UK) equipped with a Resource® Q 1 ml column (GE Healthcare) at a flow rate of 4 mL/min to obtain PEG conjugated with DTPA (DTPA-PEG). Tris-HCl buffer (20 mM, pH 9.0) was used as a running buffer, and DTPA-PEG was eluted using an NaCl concentration gradient (linear gradient of 0–1 M NaCl, 0–16 min). The elution of DTPA-PEG was confirmed by both PEG quantification and measurement of its absorbance at 254 nm for the quantitation of *p*-SCN-Bn-DTPA. The PEG concentration was determined as previously reported [21,22]. In brief, a PEG standard sample (1–20 μg/mL, 200 μL) or DTPA-PEG (200 μL) was mixed with 5% barium chloride in 1 M HCl aqueous solution (100 μL) and iodine aqueous solution [1.66% potassium iodide and 1.27% iodine in distilled deionized water (5 μL)] in a 96-well

plate for 5 min, and their absorbance values at 535 nm were measured with an Infinite® 200 PRO plate reader (Tecan Japan Co., Ltd., Kanagawa, Japan). The PEG concentration was calculated from a standard curve obtained by plotting the absorbance value against the already-known PEG concentration. Each DTPA-PEG is hereinafter referred to as DTPA-PEG5, DTPA-PEG10, DTPA-PEG20, and DTPA-PEG40 according to the molecular weight of PEG.

For radiolabeling, the purified DTPA-PEG preparations were added to ^{111}In chloride (3.7 MBq) in 0.1 M sodium acetate (pH 6.0) and were incubated for 30 min. The radiochemical purity was analyzed by sodium dodecyl sulfate-poly(acrylamide) gel electrophoresis (SDS-PAGE, Novex® Tris-Glycine 4%–20% gel, Life Technologies Co.). Gel autoradiographic images were captured with the bioimaging analyzer BAS-5000 (Fujifilm Co., Tokyo, Japan). The radioactivity in the fractions of ^{111}In-DTPA-PEG and unbound ^{111}In were quantified using Multi Gauge V3.0 software (Fujifilm Co.). The gel was soaked in ddH_2O (100 mL) mixed with 5% barium chloride in a 1 M HCl aqueous solution (50 mL) and an iodine aqueous solution (1.66% potassium iodide and 1.27% iodine in ddH_2O, 2.5 mL) [21, 22] and then incubated at r.t. for 5–10 min to develop PEG staining.

2.2.2 ICG-PEG

PEG conjugated with ICG was prepared as fluorescence and PA imaging probes. Each mono-amino PEG (0.54 μmol in 1 mL chloroform) was mixed with ICG-Sulfo-OSu [1.08 μmol in 100 μL dimethyl sulfoxide (DMSO)] at a molar ratio of PEG:ICG = 1:2, followed by incubation at r.t. for 24 h with light shielding. After solvent evaporation, the resulting mixture was dissolved in methanol (2 mL) and dialyzed against methanol with pre-treated regenerated cellulose (RC) membrane Spectra/Por® 7 dialysis tubing (MWCO: 3.5 kDa) (Spectrum Laboratories, Inc., Rancho Dominguez, CA, USA) to remove unconjugated ICG. PEG quantification was performed as described above. To confirm the number of ICG molecules conjugated to PEG, the concentration of ICG in each ICG-PEG sample was calculated based on its absorption at 795 nm in the presence of 5% SDS using a UV-Vis-NIR system (UV-1800, Shimadzu Co., Kyoto, Japan). Each ICG-PEG is hereinafter referred to as ICG-PEG5, ICG-PEG10, ICG-PEG20, and ICG-PEG40 according to the molecular weight of PEG.

To determine chemical purity, purified ICG-PEG (100 pmol ICG) was subjected to SDS-PAGE separation. The gel was imaged with an IVIS imaging System 200 (Perkin Elmer Inc., ex/em 745/840 nm, exposure time: 1 s), and the fractions of covalently bound ICG to PEG were assessed by fluorescence intensity as previously reported [19]. Subsequently, PEG staining was performed as described above.

2.2.3 DTPA-PEG-ICG

Diamino PEG (molecular weight: 20 kDa) (1.08 μmol in 1 mL chloroform) was mixed with ICG-Sulfo-OSu (1.08 μmol in 100 μL DMSO) at a ratio of PEG:ICG = 1:1 and was incubated at r.t. for 24 h with light shielding. After solvent evaporation, the sample was dissolved in methanol (2 mL). The resulting solutions were dialyzed against methanol to remove unconjugated ICG-Sulfo-OSu. Subsequently, the solvent was evaporated, MES buffer (20 mM, pH 4.0) was added, and samples were purified using a cation exchange chromatography system equipped with a Resource® S 1 ml column (GE Healthcare) at a flow rate of 4 mL/min to remove unreacted PEG. MES buffer (20 mM, pH 4.0) was used as a running buffer, and elution of PEG conjugated with ICG was performed using an NaCl concentration gradient (linear gradient of 0–1 M NaCl, 0–16 min). After buffer exchange to a borate buffer (50 mM, pH 8.5) using an Amicon Ultra centrifugal unit (MWCO: 10 kDa), DTPA anhydride (10 μmol) was added to PEG-ICG [1.08 μmol in 1 mL borate buffer (50 mM, pH 8.5)] at a reaction ratio of DTPA:PEG = 10:1, followed by incubation at 37°C for 24 h. The mixture was then ultrafiltered with an Amicon Ultra centrifugal unit (MWCO: 10 kDa) to remove any unbound DTPA. PEG conjugated with ICG and DTPA (DTPA-PEG20-ICG) was purified with an anion exchange chromatography system under the same conditions that were used for DTPA-PEG purification. DTPA-PEG20-ICG elution was confirmed by both PEG quantification and measurement of absorbance at 795 nm for the quantitation of ICG.

For radiolabeling, the purified DTPA-PEG20-ICG preparations were added to ^{111}In chloride (3.7 MBq) in 0.1 M sodium acetate (pH 6.0) and then incubated for 30 min. The radiochemical purity was analyzed as described in section 2.2.1.

2.3 In vivo biodistribution study

2.3.1 ^{111}In-DTPA-PEG

Colon 26 (mouse rectal cancer cell) tumor-bearing mice were prepared as reported previously [19]. Aminal studies were performed according to the institutional guidelines of Kyoto University, and the experimental procedures were approved by the Kyoto University Animal Care Committee. Each ^{111}In-DTPA-PEG (37 kBq, 150 μL PBS) was intravenously injected into the colon26 tumor-bearing mice (n = 3–4 for each probe at each time point). At 1, 3, 6, 24, 48, and 72 h after administration, the mice were sacrificed, and whole-organ specimens were immediately removed and weighed, and the radioactivity was measured with a NaI well-type scintillation counter (1480WIZARD, PerkinElmer Co., Waltham, MA, USA). Feces and urine were collected for 24 h after administration. The data were expressed as the percentage injected dose per gram of tissue (%ID/g) or %ID (for feces and urine).

2.3.2 ICG-PEG

The accumulation of ICG-PEG in the tumor was measured as reported previously [19]. Briefly, each ICG-PEG (13 nmol ICG in 100 μL PBS) was intravenously injected into the colon26 tumor-bearing nude mice (n = 3 for each probe at each time point). At 3, 6, 24, 48, 72, and 168 h after administration of ICG-PEGs, the tumors were excised and homogenized in a 1% triton-X aqueous solution, and the fluorescence intensity was measured. Time points were determined based on biodistribution study of ^{111}In-DTPA-PEG, and 168 h was added to investigate the excretion from organs of probe. To quantify the concentration of ICG-PEG in the blood (%ID/g), the mouse blood (2 μL) was collected at 5, 15, and 30 min and again at 1, 3, 6, 24, 48, 72, and 168 h post-injection of each ICG-PEG. Then the blood was mixed with a 1% triton-X aqueous solution (9 μL) and DMSO (9 μL), and the fluorescence intensity was measured. The concentration of ICG-PEG in the tumor and blood was calculated using a standard curve prepared from ICG-PEG diluted with mouse tumor homogenate and mouse blood, respectively. *In vivo* fluorescence images were also acquired at 3, 6, 24, 48, 72, and 168 h after administration of ICG-PEG20 using the IVIS imaging system 200 (ex/em 745/840 nm, exposure time 1 sec). Fluorescent intensity of tumor region was measured at each time point.

2.3.3 ^{111}In-DTPA-PEG20-ICG

Biodistribution studies using ^{111}In-DTPA-PEG20-ICG were performed as described in section 2.3.1. *In vivo* biodistribution was monitored at 1, 3, 6, 24, 48, and 72 h after probe injection. Time points were determined based on biodistribution study of ^{111}In-DTPA-PEG.

2.4 Protein binding assay

The binding affinities of PEG derivatives to albumin were measured as reported previously [23]. Briefly, ICG-PEG20 (0–60 μM), ICG (0–14 μM), In-DTPA-PEG20 (0–50 μM), or PEG20 (0–50 μM) was incubated with bovine serum albumin (BSA) (4 μM) for 30 min to equilibrate. The fluorescence intensity of tryptophan in BSA was measured using a spectrofluorophotometer (RF-5300PC, Shimadzu Co., ex/em 279/342 nm). The binding affinity of each compound to BSA was calculated from the Hill equation expressed by Eq (1) for a static quenching interaction.

$$\log [(F_0\text{-}F)/F] = \log K_b + n \log [ICG] \quad (1)$$

Where K_b is the binding constant, n is the number of binding sites, and F and F_0 are the fluorescence intensities of tryptophan of BSA with and without each compound, respectively.

2.5 In vivo imaging study

2.5.1 SPECT study

^{111}In-DTPA-PEG20 (molecular weight: 20 kDa, 21 MBq, 150 μL PBS) were intravenously injected into the colon26 tumor-bearing mice (n = 3). The mice were anesthetized by isoflurane, and SPECT and CT images were obtained using the U-SPECT-II system (MILabs, Utrecht, the Netherlands) with 0.6-mm pinhole collimators (SPECT conditions: 30 min × 1 frame; CT conditions: accurate full angle mode in 65 kV/615 μA) at 24 h after injection of ^{111}In-DTPA-PEG20. SPECT images were reconstructed using the OSEM method (6 subset, 1 iteration) with a 0.6-mm Gaussian filter.

2.5.2 In vivo PA imaging

In vivo PA imaging was performed with an Endra Life Sciences Nexus 128 instrument (Endra Inc., Ann Arbor, MI, USA) as reported previously [19]. ICG-PEG20 (13, 26, 52, and 104 nmol ICG in 100 μL PBS) was intravenously injected into colon26 tumor-bearing mice (n = 3). PA images of tumor and non-tumor (back) regions were acquired (120 angles,100 pulses per angle with a 797 nm pulsed laser) before injection and at 24 h after injection. After PA image reconstruction, PA signal intensity was analyzed using Osirix after normalization to the irradiated laser intensity.

2.6 Statistical analysis

Each experiment was performed at least three times. Three to four mice were used for *in vivo* experiments. The statistical significance of differences between groups was determined using the Student's *t*-test (two-tailed). Data are presented as the mean ± standard deviation. Differences at the 95% confidence level ($P < 0.05$) were considered significant.

3. Results

3.1 Probe synthesis

The hydrodynamic diameter of each monoamino PEG was 4.4 ± 0.03, 6.3 ± 0.05, 9.3 ± 0.04, and 13.6 ± 0.2 nm for PEG5, PEG10, PEG20, and PEG40, respectively. PEG-based probes were synthesized according to the schemes summarized in Fig. 1. The high radiochemical purity of ^{111}In-labeled DTPA-PEG was demonstrated by autoradiographic analysis of SDS-PAGE (Fig. 2: 95.7 ± 0.7, 98.7 ± 1.0, 96.6 ± 0.3, and 96.5 ± 0.1% for ^{111}In-DTPA-PEG5, ^{111}In-DTPA-PEG10, ^{111}In-DTPA-PEG20, and ^{111}In-DTPA-PEG40, respectively).

The conjugation ratios of ICG to PEG were ≈1 for each ICG-PEG conjugate (1.03 ± 0.01, 0.93 ± 0.02, 0.99 ± 0.02, and 1.03 ± 0.01 for ICG-PEG5, ICG-PEG10, ICG-PEG20, and ICG-PEG40, respectively). As defined by SDS-PAGE analysis, the fractions of covalently bound ICG to PEG were 98.3 ± 0.2%, 99.0± 0.4%, 99.4 ± 0.1%, and 99.4 ± 0.1% for ICG-PEG5,

ICG-PEG10, ICG-PEG20, and ICG-PEG40, respectively (Fig. 3). The radiochemical purity of ^{111}In-DTPA-PEG20-ICG was 95.2 ± 1.5%.

3.2 In vivo biodistribution study

3.2.1 ^{111}In-DTPA-PEGs

The results of the *in vivo* biodistribution studies for ^{111}In-DTPA-PEG at 1, 3, 6, 24, 48, and 72 h after administration were summarized in Table 1. As the molecular weight of PEG increased, its half-life in the blood was prolonged (0.1, 0.2, 4.5, and 10.6 %ID/g at 24 h post-injection for ^{111}In-DTPA-PEG5, ^{111}In-DTPA-PEG10, ^{111}In-DTPA-PEG20, and ^{111}In-DTPA-PEG40, respectively). For ^{111}In-DTPA-PEG5 and ^{111}In-DTPA-PEG10, the highest tumor uptake was observed 1 h after administration (0.6 and 1.5 %ID/g for ^{111}In-DTPA-PEG5 and ^{111}In-DTPA-PEG10, respectively) and then there was a gradual decrease by 3 h. On the other hand, ^{111}In-DTPA-PEG20 and ^{111}In-DTPA-PEG40 both showed the highest accumulation in the tumor among tissues excised at 24 h after administration (6.2 and 12.9 %ID/g for ^{111}In-DTPA-PEG20 and ^{111}In-DTPA-PEG40, respectively). Although the accumulation of each ^{111}In-DTPA-PEG in normal tissues, including the kidneys, liver, spleen, and skin was also observed, these uptake levels were not notable, and they were mainly excreted into the urine until 24 h after injection (40.0, 44.1, 42.4, and 14.7 %ID for ^{111}In-DTPA-PEG5, ^{111}In-DTPA-PEG10, ^{111}In-DTPA-PEG20, and ^{111}In-DTPA-PEG40, respectively). The ^{111}In-DTPA-PEG tumor-to-blood ratios increased with time, exceeding 1.0 at 24 h post-injection for ^{111}In-DTPA-PEG20 and ^{111}In-DTPA-PEG40.

Table 1

In vivo biodistribution of ^{111}In-DTPA-PEG in colon26 tumor-bearing mice at 1, 3, 6, 24, 48, and 72 h after administration. [a]

Organs (%ID/g) and excreta (%ID)	^{111}In-DTPA-PEG5					
	1 h	3 h	6 h	24 h	48 h	72 h
Blood	0.5 ± 0.1	0.3 ± 0.4	0.2 ± 0.0	0.1 ± 0.0	0.1 ± 0.0	0.1 ± 0.0
Heart	0.8 ± 0.8	0.1 ± 0.0	0.2 ± 0.0	0.2 ± 0.0	0.1 ± 0.0	0.2 ± 0.0
Lungs	0.9 ± 0.6	0.2 ± 0.0	0.2 ± 0.0	0.2 ± 0.0	0.1 ± 0.0	0.2 ± 0.0
Liver	0.3 ± 0.1	0.2 ± 0.1	0.2 ± 0.0	0.2 ± 0.0	0.1 ± 0.0	0.2 ± 0.0
Kidneys	2.2 ± 0.2	1.4 ± 0.2	1.4 ± 0.1	1.2 ± 0.1	0.7 ± 0.0	0.7 ± 0.1
Stomach	0.6 ± 0.2	0.7 ± 0.3	0.3 ± 0.1	0.4 ± 0.2	0.2 ± 0.1	0.4 ± 0.1
Intestine	0.3 ± 0.2	1.1 ± 0.8	0.4 ± 0.3	0.3 ± 0.1	0.1 ± 0.0	0.4 ± 0.1
Pancreas	0.3 ± 0.1	0.2 ± 0.1	0.1 ± 0.0	0.1 ± 0.0	0.1 ± 0.0	0.1 ± 0.0
Spleen	0.3 ± 0.1	0.1 ± 0.0	0.4 ± 0.1	0.3 ± 0.2	0.1 ± 0.0	0.6 ± 0.7
Muscle	0.5 ± 0.3	0.2 ± 0.1	0.2 ± 0.0	0.2 ± 0.0	0.1 ± 0.0	0.1 ± 0.1
Skin	1.0 ± 0.4	0.5 ± 0.3	0.3 ± 0.1	0.2 ± 0.1	0.1 ± 0.0	0.2 ± 0.1

Tumor	0.6	±	0.1	0.5	±	0.2	0.4	±	0.1	0.4	±	0.0	0.2	±	0.0	0.2	±	0.0
Tumor/blood ratio	1.1	±	0.2	2.8	±	1.8	2.6	±	0.9	4.2	±	0.7	4.4	±	1.1	3.5	±	0.7
Feces										13.9	±	4.2						
Urine										40.0	±	11.8						

Organs (%ID/g) and excreta (%ID)	**^{111}In-DTPA-PEG10**																	
	1 h			**3 h**			**6 h**			**24 h**			**48 h**			**72 h**		
Blood	3.3	±	0.6	0.8	±	0.1	0.8	±	0.1	0.2	±	0.0	0.1	±	0.0	0.1	±	0.0
Heart	1.0	±	0.1	0.2	±	0.0	0.3	±	0.0	0.2	±	0.0	0.1	±	0.0	0.3	±	0.1
Lungs	1.5	±	0.4	0.3	±	0.1	0.5	±	0.1	0.3	±	0.0	0.2	±	0.0	0.3	±	0.0
Liver	0.9	±	0.1	0.7	±	0.2	0.6	±	0.0	0.5	±	0.1	0.3	±	0.0	0.3	±	0.0
Kidneys	2.7	±	0.4	1.6	±	0.2	1.7	±	0.1	1.5	±	0.2	0.8	±	0.1	0.7	±	0.2
Stomach	0.9	±	0.3	0.8	±	0.2	0.5	±	0.2	0.5	±	0.3	0.2	±	0.0	0.3	±	0.1
Intestine	0.7	±	0.1	0.8	±	0.4	0.7	±	0.3	0.6	±	0.4	0.2	±	0.0	0.2	±	0.0
Pancreas	0.8	±	0.2	0.3	±	0.1	0.3	±	0.0	0.3	±	0.0	0.2	±	0.0	0.2	±	0.1
Spleen	0.7	±	0.2	0.3	±	0.1	0.5	±	0.2	0.6	±	0.4	0.3	±	0.0	0.4	±	0.1
Muscle	1.0	±	0.1	0.3	±	0.0	0.3	±	0.1	0.2	±	0.0	0.2	±	0.0	0.2	±	0.0
Skin	2.2	±	0.4	0.9	±	0.1	0.8	±	0.2	0.6	±	0.0	0.4	±	0.1	0.4	±	0.0
Tumor	1.5	±	0.1	1.4	±	0.3	1.2	±	0.2	1.1	±	0.3	0.5	±	0.1	0.4	±	0.0
Tumor/blood ratio	0.5	±	0.1	1.6	±	0.4	1.6	±	0.0	6.0	±	0.7	8.7	±	1.3	5.1	±	1.6
Feces										10.3	±	7.1						
Urine										44.1	±	12.9						

Organs (%ID/g) and excreta (%ID)	**^{111}In-DTPA-PEG20**																	
	1 h			**3 h**			**6 h**			**24 h**			**48 h**			**72 h**		
Blood	22.7	±	1.4	11.3	±	1.0	10.8	±	0.2	4.5	±	0.6	3.7	±	0.1	1.9	±	0.5
Heart	3.9	±	0.2	2.5	±	0.2	2.1	±	0.3	1.2	±	0.1	1.4	±	0.0	1.1	±	0.2
Lungs	5.5	±	0.7	3.1	±	0.4	3.1	±	0.2	1.6	±	0.2	1.4	±	0.0	1.4	±	0.2
Liver	4.5	±	0.4	3.3	±	0.3	3.7	±	0.7	2.7	±	0.5	2.9	±	0.1	3.0	±	0.4
Kidneys	9.4	±	0.3	6.5	±	0.2	6.0	±	0.2	3.8	±	0.4	3.6	±	0.1	2.9	±	0.4
Stomach	2.8	±	0.2	2.8	±	0.4	2.2	±	0.9	0.5	±	0.1	0.6	±	0.2	0.7	±	0.1
Intestine	2.9	±	0.2	1.9	±	0.1	1.7	±	0.2	0.6	±	0.1	0.5	±	0.0	0.5	±	0.1
Pancreas	3.5	±	0.5	2.3	±	0.1	1.9	±	0.0	1.1	±	0.2	1.6	±	0.3	1.3	±	0.2
Spleen	3.2	±	0.2	2.0	±	0.3	2.1	±	0.1	2.0	±	0.5	2.2	±	0.1	2.6	±	0.7
Muscle	1.1	±	0.1	1.6	±	0.2	1.2	±	0.3	0.7	±	0.2	0.5	±	0.1	0.7	±	0.1
Skin	2.6	±	0.4	3.8	±	1.0	2.5	±	0.4	2.2	±	0.3	2.4	±	0.6	2.8	±	0.2
Tumor	2.9	±	0.3	4.2	±	0.1	5.0	±	1.0	6.2	±	0.7	5.4	±	0.7	5.5	±	1.3
Tumor/blood ratio	0.1	±	0.0	0.4	±	0.0	0.5	±	0.1	1.4	±	0.2	1.4	±	0.2	2.8	±	0.1
Feces										6.7	±	2.6						
Urine										42.4	±	10.0						

Organs (%ID/g) and excreta (%ID)	**^{111}In-DTPA-PEG40**																	
	1 h			**3 h**			**6 h**			**24 h**			**48 h**			**72 h**		
Blood	43.9	±	1.4	31.5	±	3.2	29.0	±	1.9	10.6	±	1.4	5.2	±	0.5	2.8	±	0.5
Heart	5.0	±	0.8	4.3	±	0.3	4.1	±	0.3	2.3	±	0.3	1.6	±	0.1	1.5	±	0.1
Lungs	9.7	±	2.7	6.2	±	0.7	6.2	±	0.8	3.5	±	0.5	2.1	±	0.2	2.0	±	0.0

Liver	8.0	±	1.8	5.5	±	0.9	7.2	±	1.3	4.0	±	0.6	3.3	±	0.3	3.2	±	0.2
Kidneys	11.1	±	1.6	10.2	±	0.7	8.9	±	1.1	5.0	±	0.4	3.4	±	0.4	2.7	±	0.2
Stomach	2.6	±	0.5	3.3	±	0.5	3.3	±	0.2	2.0	±	0.5	1.2	±	0.2	1.0	±	0.1
Intestine	2.3	±	0.1	2.3	±	0.0	2.3	±	0.3	1.4	±	0.1	0.8	±	0.1	0.6	±	0.0
Pancreas	3.7	±	0.7	3.7	±	0.3	4.7	±	0.1	3.8	±	0.6	3.1	±	0.2	3.0	±	0.2
Spleen	3.9	±	0.5	4.1	±	0.5	4.2	±	0.7	3.9	±	1.0	4.0	±	0.4	4.1	±	0.4
Muscle	1.1	±	0.3	1.4	±	0.1	1.7	±	0.1	1.5	±	0.1	1.3	±	0.1	1.7	±	0.2
Skin	2.1	±	0.2	3.4	±	0.4	4.5	±	0.3	4.9	±	0.4	4.6	±	0.2	6.2	±	0.5
Tumor	3.0	±	0.7	4.4	±	0.4	7.6	±	1.0	12.9	±	1.6	12.3	±	1.0	10.5	±	1.9
Tumor/blood ratio	0.1	±	0.0	0.1	±	0.0	0.3	±	0.0	1.2	±	0.0	2.4	±	0.2	3.8	±	0.5
Feces										4.7	±	1.3						
Urine										14.7	±	3.9						

[a] Results are expressed as the mean ± SD (n = 3–4).

3.2.2 In vivo biodistribution of ICG-PEG conjugate

The accumulation of ICG-PEG in the excised tumors and blood was determined based on the ICG fluorescence intensity (Fig. 4). ICG-PEG20 and ICG-PEG40 showed a higher accumulation in the tumor tissue (Fig. 4A) and a longer half-life in circulation (Fig. 4B) than ICG-PEG5, ICG-PEG10, and ICG alone. The highest accumulation in the tumor tissue was observed at 24 h for ICG-PEG20 (14.9 ± 1.2 %ID/g) and at 48 h for ICG-PEG40 (20.6 ± 1.7 %ID/g). The circulation half-lives for ICG, ICG-PEG5, ICG-PEG10, ICG-PEG20, and ICG-PEG40 were 0.098, 0.57, 1.24, 9.5, and 22.5 h, respectively. The tumor-to-blood ratios for ICG-PEG20 and ICG-PEG40 at 24 h post-injection were 1.2 ± 0.1 and 0.7 ± 0.1, respectively.

Although there was a difference in the *in vivo* biodistribution of ^{111}In-DTPA-PEG and ICG-PEG, particularly in tumor uptake, their time-dependent uptake pattern was similar. At 24 h after injection, T/B ratios of ^{111}In-DTPA-PEG5 and PEG10 were significantly higher than PEG20 and PEG40; however, their absolute accumulation was below the sensitivity of the *in vivo* imaging system. On the other hand, PEG20 and PEG40 showed the highest accumulation in the tumor tissue from among the tissues excised at 24 or 48 h post-injection. Furthermore, PEG20 exhibited a relatively higher tumor-to-blood ratio at 24 h post-injection; therefore, ICG-PEG20 was investigated in an additional *in vivo* imaging study. Whole body fluorescence images of tumor-bearing mice administrated with ICG-PEG20 were shown in Fig. 5 (fluorescence image data of ICG, ICG-PEG5, ICG-PEG10, and ICG-PEG40 were summarized in Supplementary material, Fig S1). Tumors inoculated in the right shoulders were clearly detected at 24 h after administration (Fig. 5A). The time-dependent change of fluorescence signal intensity in tumor region was consistent with the data of *in vivo* biodistribution study using ICG-PEG20 (Fig. 4A and Fig. 5B).

3.2.3 In vivo biodistribution of ^{111}In-DTPA-PEG20-ICG conjugate

Compared to ^{111}In-DTPA-PEG, ICG-PEG showed a prolonged half-life in circulation (4.5 and 12.8 %ID/g at 24 h post injection for ^{111}In-DTPA-PEG20 and ICG-PEG20, respectively) and higher accumulation in the tumor tissue. To determine the differences in pharmacokinetics between ^{111}In-DTPA-PEG and ICG-PEG, PEG20 labeled with both ^{111}In and ICG was prepared (Supplementary material, Fig. S2 and S3), and its *in vivo* biodistribution was evaluated at 1, 6, 24, and 72 h after administration (Table 2). Among the organs excised 24 h after administration, the highest accumulation of ^{111}In-DTPA-PEG20-ICG was observed in the tumor tissue (11.1 %ID/g), which was consistent with the results of the fluorescence measurement study using ICG-PEG20 (Fig. 4). The radioactivity of ^{111}In-DTPA-PEG20-ICG and ICG-PEG20 in the blood (9.0 ± 0.5 and 12.8 ± 2.3 %ID/g at 24 h, respectively) was more than two-fold higher than ^{111}In-DTPA-PEG20 (4.5 ± 0.6 %ID/g at 24 h). Although the main excretion pathway of ^{111}In-DTPA-PEG20-ICG was through the urine (Table 2), the urinary excretion of ^{111}In-DTPA-PEG20-ICG (24.6%) was significantly lower than that of ^{111}In-DTPA-PEG20 (42.4%) ($P < 0.05$), suggesting that the introduction of ICG can reduce urinary excretion, resulting in the prolongation of ICG-PEG20 blood clearance. The tumor-to-blood ratios of ^{111}In-DTPA-PEG20-ICG were comparable to those of ^{111}In-DTPA-PEG20 and ICG-PEG20.

Table 2

In vivo biodistribution of ^{111}In-DTPA-PEG20-ICG in colon26 tumor-bearing mice.[a]

Organs (%ID/g) and excreta (%ID)	^{111}In-DTPA-PEG20-ICG					
	1 h	3 h	6 h	24 h	48 h	72 h
Blood	35.6 ± 4.7	28.2 ± 2.0	21.9 ± 2.5	9.0 ± 0.5	5.4 ± 0.4	1.6 ± 0.4
Heart	4.9 ± 0.6	4.3 ± 1.1	3.4 ± 0.3	2.6 ± 0.1	2.6 ± 0.2	1.7 ± 0.2
Lungs	7.7 ± 1.6	7.6 ± 1.5	5.0 ± 0.5	3.1 ± 0.3	2.7 ± 0.3	1.8 ± 0.2
Liver	8.3 ± 0.9	8.7 ± 0.1	8.2 ± 0.7	8.7 ± 0.44	8.1 ± 0.7	8.5 ± 0.4
Kidneys	10.3 ± 0.4	9.0 ± 0.8	8.2 ± 0.3	7.1 ± 0.6	5.8 ± 0.5	4.1 ± 0.5
Stomach	1.3 ± 0.2	1.9 ± 0.1	0.9 ± 0.3	1.1 ± 0.6	1.8 ± 0.4	0.9 ± 0.2
Intestine	2.4 ± 0.2	2.2 ± 0.3	1.6 ± 0.2	1.6 ± 0.2	1.7 ± 0.1	1.1 ± 0.1
Pancreas	3.9 ± 0.1	2.7 ± 0.1	2.8 ± 0.2	2.3 ± 0.3	2.3 ± 0.3	2.0 ± 0.2
Spleen	4.4 ± 0.1	4.9 ± 0.9	3.8 ± 0.4	4.6 ± 0.6	5.2 ± 0.5	4.5 ± 0.4
Muscle	1.0 ± 0.1	1.2 ± 0.2	1.0 ± 0.2	1.2 ± 0.1	1.5 ± 0.0	1.4 ± 0.4
Skin	2.1 ± 0.3	2.3 ± 0.3	2.9 ± 0.5	4.1 ± 0.5	5.4 ± 0.7	5.1 ± 0.2
Tumor	2.9 ± 0.2	5.5 ± 1.5	5.1 ± 0.1	11.1 ± 0.5	10.2 ± 3.0	7.2 ± 0.6
Tumor/blood ratio	0.1 ± 0.0	0.2 ± 0.0	0.2 ± 0.0	1.2 ± 0.1	1.9 ± 0.7	4.7 ± 0.6
Feces				3.5 ± 2.2		
Urine				24.6 ± 3.2		

[a] Results are expressed as mean ± SD %ID/g (n=3–4).

3.3 Protein binding assay

To investigate the basis for reduced urinary excretion with ICG conjugation to PEG, we evaluated the interaction between ICG and blood proteins (BSA) (Fig. 6). ICG itself strongly bound to albumin, and the binding affinity (5.2×10^5 M^{-1}) was generally consistent with previous reports [23]. ICG-PEG20 also exhibited affinity to albumin (1.4×10^5 M^{-1}), although the binding affinity was lower than ICG itself. On the other hand, In-DTPA-PEG20 and PEG20 did not show any binding affinity to albumin.

3.4 In vivo imaging study

3.4.1 SPECT/CT study

SPECT images of tumor-bearing mice at 24 h after administration with ^{111}In-DTPA-PEG20 are shown in Fig. 7. The tumors inoculated in the right shoulders were clearly visualized with high background ratios. Weak ^{111}In-DTPA-PEG20 signals were detected in the liver and kidneys.

3.4.2 In vivo photoacoustic imaging study

The feasibility of ICG-PEG as a tumor-targeted PA imaging probe was evaluated. Prior to the *in vivo* study, the comparable PA signal intensity of ICG-PEG conjugates to that of ICG was confirmed (Supplementary material, Fig. S4).

For mice set in the PA imaging instrument as shown in Fig. 8A, a slight PA signal derived from hemoglobin in the blood was observed at the tumor and non-tumor regions before probe injection (Fig. 8B-F). ICG-PEG20 (13 nmol or more) clearly visualized the tumor 24 h post-injection (Fig. 8B-E). On the other hand, a subtle increase of PA signal was observed in the non-tumor region when ICG-PEG20 (26 nmol ICG) was administered (a 30% increase compared to pre-injection, Fig. 8F). The PA signal in the tumor region increased in proportion with the injected dose of ICG-PEG20 within the range of measurement [14 ± 48, 152 ± 72, 359 ± 81, and 715 ± 205% increase compared to pre-injection for 13, 26, 52, and 104 nmol ICG (ICG-PEG20), respectively] (Fig. 9).

4. Discussion

In this study, we synthesized new ^{111}In-labeled PEGs and ICG-labeled PEGs with different molecular weights and evaluated both their quantitative *in vivo* biodistribution and their potential as diagnostic drug carriers for tumor imaging.

The tumor uptake of ^{111}In-DTPA-PEG and ICG-PEG increased with increasing PEG molecular weight due to prolonged retention of the larger PEG molecules in circulation,

which may enhance the opportunity for tumor uptake through an EPR effect. The relationship between the PEG molecular weight and its half-life in circulation has been reported using iodine-125-labeled PEG [24], which was mostly consistent with our data. The circulation half-life of ^{111}In-DTPA-PEG with 20 kDa PEG or greater was dramatically extended compared to PEG5 and PEG10. It is well established that hydrophilic PEG can be hydrated, resulting in the enlargement of its apparent size compared with a protein of similar molecular weight [25]. When calculated on the basis of the formula reported by Fee and Van Alstine [26], the hydrodynamic diameters of PEG5, PEG10, PEG20, and PEG40 are 4.5, 6.6, 9.7, and 14.3 nm, respectively. These values were in good agreement with size measured by DLS (4.4, 6.3, 9.3, and 13.6 nm for PEG5, PEG10, PEG20, and PEG40, respectively). A protein or nanoparticle with a hydrodynamic diameter of ~6–8 nm is considered to be cleared rapidly because of renal clearance through glomerular filtration in the kidney [27,28]. Because PEG5 and PEG10 are smaller than this filtration size, they were rapidly eliminated from the blood to the urine (Table 1). Even ^{111}In-DTPA-PEG20 and ^{111}In-DTPA-PEG40, with hydrodynamic diameters greater than the limitation of glomerular filtration, were largely excreted in urine. This finding is probably the result of a linear water-soluble polymer passing through the renal filter by a snake-like movement, unlike a spherical molecule [29]. Because of primary and rapid urinary excretion, the accumulation of ^{111}In-DTPA-PEG in normal organs, including the liver and kidney, was reduced, leading to lower tumor-to-background ratios, which may be favorable for high contrast tumor imaging (Fig. 7).

Unexpectedly, there was a divergence in biodistribution (%ID/g value) between ^{111}In-labeled PEG and ICG-labeled PEG. As shown in Tables 1, 2, and Figure 4, the addition of ICG to PEG induced a prolonged half-life of the probe in circulation, resulting in an increase in tumor uptake. ICG is known to interact with proteins (lipoprotein, globulin, and albumin) [30] and to complex itself into aggregates [31]. Because the results of the protein binding assay (Fig. 6) suggested the intense interaction of ICG-PEG with albumin, ICG-PEG bound with albumin would be excreted less into the urine, which could prolong its blood residence time. On the other hand, PEG conjugated with DTPA, a highly water-soluble chelator, did not show any interaction with BSA. Although our results indicated that the pharmacokinetics of PEG derivatives would be altered by this labeling method, ICG-PEG showed a significantly higher tumor accumulation than ^{111}In-DTPA-PEG as well as comparable tumor-to-blood ratios. ^{111}In-DTPA-PEG20-ICG also showed high tumor accumulation as well as ICG-PEG. ^{111}In-DTPA-PEG20-ICG has dual signal emitters in the structure, which could achieve SPECT and fluorescence multimodal imaging in future study.

ICG-PEG20 could clearly visualize the tumor location in fluorescence imaging (Fig. 5) and PA imaging (Fig. 8), and produced increased PA signals equal to or greater than other PA imaging agents that have been previously reported [32-35]. We confirmed its high

quantitative capability in PA imaging from the results of the PA signal increase proportional to the injected dose (Fig. 9). Both PEG and ICG have been FDA approved [15, 16] because of their biocompatibility [9]. There was no change in the appearance of the mice even at the highest injection dose (104 nmol) evaluated in this study. In addition, the biodistribution study using ^{111}In-labeled PEG or ICG-PEG did not show prominent accumulation in normal organs (Tables 1 and 2). Therefore, facile clinical translation of ^{111}In-labeled PEG and ICG-PEG is expected.

5. Conclusions

We confirmed the favorable characteristics of PEG derivatives as diagnostic drug carriers for cancer imaging. PEG is highly hydrophilic and was easily modified through the conjugation of a signal emitter for diagnosis. Furthermore, the PEG chain itself possessing functional group at termini (20 kDa) showed marked tumor accumulation through EPR effects with no marked accumulation in normal tissues. Both SPECT studies using ^{111}In-DTPA-PEG20 and PA imaging studies using ICG-PEG20 achieved high contrast tumor imaging, suggesting the feasibility of using PEG derivatives as diagnostic drug carriers for tumor imaging.

Acknowledgements

This work was partly supported by the Innovative Techno-Hub for Integrated Medical Bio-imaging Project of the Special Coordination Funds for Promoting Science and Technology, from the Ministry of Education, Culture, Sports, Science and Technology (MEXT), Japan. Part of this study was supported by JSPS KAKENHI Grant Number 15H04637.

References

[1] H. Cabral, K. Miyata, A. Kishimura, Nanodevices for studying nano-pathophysiology, Adv. Drug Deliv. Rev. 74 (2014) 35–52.

[2] M.S. Muthu, D.T. Leong, L. Mei, S.S. Feng, Nanotheranostics - application and further development of nanomedicine strategies for advanced theranostics, Theranostics. 4 (2014) 660–677.

[3] D.E. Owens III, N.A. Peppas, Opsonization, biodistribution, and pharmacokinetics of polymeric nanoparticles, Int. J. Pharm. 307 (2006) 93–102.

[4] H. Maeda, Tumor-selective delivery of macromolecular drugs *via* the EPR effect: background and future prospects, Bioconjugate Chem. 21 (2010) 797–802.

[5] H. Maeda, Y. Matsumura, EPR effect based drug design and clinical outlook for enhanced cancer chemotherapy, Adv. Drug Deliv. Rev. 63 (2011) 129–130.

[6] T. McDonnell, Y. Ioannou, A. Rahman, PEGylated drugs in rheumatology - why develop them and do they work? Rheumatology (Oxford) 53 (2014) 391–396.

[7] A.M. Prantner, N. Scholler, Biological barriers and current strategies for modifying nanoparticle bioavailability, J. Nanosci. Nanotechnol. 14 (2014) 115–125.

[8] G. Pasut, F.M. Veronese, State of the art in PEGylation: the great versatility achieved after forty years of research, J. Control. Release 161 (2012) 461–472.

[9] C. Fruijtier-Pölloth, Safety assessment on polyethylene glycols (PEGs) and their derivatives as used in cosmetic products, Toxicology 214 (2005) 1–38.

[10] F.F. Davis., The origin of pegnology, Adv. Drug Deliv. Rev. 54 (2002) 457–458.

[11] C. Kim, T. N. Erpelding, L. Jankovic, M. D. Pashley, L. V. Wang, Deeply penetrating *in vivo* photoacoustic imaging using a clinical ultrasound array system, Biomed. Opt. Express 1 (2010) 278-284.

[12] A. Horiguchi, K. Tsujita, K. Irisawa, T. Kasamatsu, K. Hirota, M. Kawaguchi, M. Shinchi, K. Ito, T. Asano, H. Shinmoto, H. Tsuda, M. Ishihara, A pilot study of photoacoustic imaging system for improved real-time visualization of neurovascular bundle during radical prostatectomy, Prostate. Published online 2015 Oct 23. Articles in Press. doi: 10.1002/pros.23122.

[13] G. Ku, L.V. Wang, Deeply penetrating photoacoustic tomography in biological tissues enhanced with an optical contrast agent, Opt. Lett. 30 (2005) 507–509.

[14] V. Ntziachristos, Going deeper than microscopy: the optical imaging frontier in biology, Nat. Methods 7 (2010) 603–614.

[15] V.L. Dzurinko, A.S. Gurwood, J.R. Price, Intravenous and indocyanine green angiography, Optometry 75 (2004) 743–755.

[16] S.G. Sakka, Assessing liver function, Curr. Opin. Crit. Care 13 (2007) 207–214.

[17] G.R. Cherrick, S.W. Stein, C.M. Leevy, C.S. Davidson, Indocyanine green: observations on its physical properties, plasma decay, and hepatic extraction, J. Clin. Invest. 39 (1960) 592–600.

[18] A. de la Zerda, S. Bodapati, R. Teed, S.Y. May, S.M. Tabakman, Z. Liu, B.T. Khuri-Yakub, X. Chen, H. Dai, S.S. Gambhir, Family of enhanced photoacoustic imaging agents for high-sensitivity and multiplexing studies in living mice, ACS Nano 6 (2012) 4694–4701.

[19] K. Kanazaki, K. Sano, A. Makino, A. Takahashi, J. Deguchi, M. Ohashi, T. Temma, M. Ono, H. Saji, Development of human serum albumin conjugated with near-infrared dye for photoacoustic tumor imaging, J. Biomed. Opt. 19 (2014) 96002.

[20] G. Kim, S.W. Huang, K.C. Day, M. O'Donnell, R.R. Agayan, M.A. Day, R. Kopelman, S. Ashkenazi, Indocyanine-green-embedded PEBBLEs as a contrast agent for photoacoustic imaging, J. Biomed. Opt. 12 (2007) 044020.

[21] G.E. Sims, T.J. Snape, A method for the estimation of polyethylene glycol in plasma protein fractions, Anal. Biochem. 107 (1980) 60–63.

[22] M.F. Zambaux, F. Bonneaux, R. Gref, E. Dellacherie, C. Vigneron, Protein C-loaded monomethoxypoly (ethylene oxide)-poly(lactic acid) nanoparticles, Int. J. Pharm. 212 (2001) 1–9.

[23] M.Y. Berezin, K. Guo, W. Akers, J. Livingston, M. Solomon, H. Lee, K. Liang, A. Agee, S. Achilefu, Rational approach to select small peptide molecular probes labeled with fluorescent cyanine dyes for *in vivo* optical imaging, Biochemistry 50 (2011) 2691–2700.

[24] T. Yamaoka, Y. Tabata, Y. Ikada, Distribution and tissue uptake of poly(ethylene glycol) with different molecular weights after intravenous administration to mice, J. Pharm. Sci. 83 (1994) 601–606.

[25] J.M. Harris, R.B. Chess, Effect of pegylation on pharmaceuticals, Nat. Rev. Drug Discov. 2 (2003) 214–221.

[26] C.J. Fee, J.M. Van Alstine, Prediction of the viscosity radius and the size exclusion chromatography behavior of PEGylated proteins, Bioconjugate chem. 15 (2004) 1304–1313.

[27] J. Liu, M. Yu, C. Zhou, J. Zheng, Renal clearable inorganic nanoparticles: a new frontier of bionanotechnology, Material Today 16 (2013) 477–486.

[28] H.S. Choi, W. Liu, P. Misra, E. Tanaka, J.P. Zimmer, B. Itty Ipe, M.G. Bawendi, J.V. Frangioni, Renal clearance of quantum dots, Nature Biotechnol. 25 (2007) 1165–1170.

[29] F.M. Veronese, G. Pasut, PEGylation, successful approach to drug delivery, Drug Discov. Today 10 (2005) 1451–1458.

[30] C. Colyer, Noncovalent labeling of proteins in capillary electrophoresis with laser-induced fluorescence detection, Cell Biochem. Biophys. 33 (2000) 323–337.

[31] H.V. Berlepsch, C. Böttcher, Cryo-transmission electron microscopy reveals mesoscopic H- and J-aggregates of near infrared cyanine dyes, J. Photochem. Photobiol. A: Chemistry 214 (2010) 16–21.

[32] P.C. Li, C.R. Wang, D.B. Shieh, C.W. Wei, C.K. Liao, C. Poe, S. Jhan, A.A. Ding, Y.N. Wu, *In vivo* photoacoustic molecular imaging with simultaneous multiple selective targeting using antibody-conjugated gold nanorods, Opt. Express 16 (2008) 18605–18615.

[33] A. de la Zerda, Z. Liu, S. Bodapati, R. Teed, S. Vaithilingam, B.T. Khuri-Yakub, X. Chen, H. Dai, S.S. Gambhir, Ultrahigh sensitivity carbon nanotube agents for photoacoustic molecular imaging in living mice, Nano Lett. 10 (2010) 2168–2172.

[34] K. Cheng, S.R. Kothapalli, H. Liu, A.L. Koh, J.V. Jokerst, H. Jiang, M. Yang, J. Li, J. Levi, J.C. Wu, S.S. Gambhir, Z. Cheng, Construction and validation of nano gold tripods for molecular imaging of living subjects, J. Am. Chem. Soc. 136 (2014) 3560–3571.

[35] K. Sano, M. Ohashia, K. Kanazaki, N. Ding, J. Deguchi, Y. Kanada, M. Ono, H. Saji, *In vivo* photoacoustic imaging of cancer using indocyanine green-labeled monoclonal antibody targeting the epidermal growth factor receptor, Biochem. Biophys. Res. Commun. 464 (2015) 820–825.

Figure legends

Fig. 1. Reaction scheme of probe synthesis. (A) ^{111}In-DTPA-PEG, (B) ICG-PEG, (C) ^{111}In-DTPA-PEG-ICG.

Fig. 2. Electrophoretic analysis of ^{111}In-DTPA-PEG. Autoradiographic images of ^{111}In-DTPA-PEG after electrophoresis (left panel) and after iodine staining to detect PEG (right panel). Lane content: 1, ^{111}In only; 2, ^{111}In-DTPA-PEG5; 3, ^{111}In-DTPA-PEG10; 4, ^{111}In-DTPA-PEG20; 5, ^{111}In-DTPA-PEG40.

Fig. 3. Electrophoretic analysis of ICG-PEG. Fluorescent images of ICG-PEGs after electrophoresis (left panel) and after iodine staining to detect PEG (right panel). Lane content: 1, ICG-sulfo-OSu; 2, ICG-PEG5; 3, ICG-PEG10; 4, ICG-PEG20; 5, ICG-PEG-40.

Fig. 4. Measurement of the *in vivo* fluorescence of colon26 tumor-bearing mice injected with ICG-PEGs and ICG alone. The graph presents the time course for the accumulation of ICG-PEGs or ICG (%ID/g) in the tumor (A) and blood (B).

Fig. 5. *In vivo* fluorescence imaging of colon26 tumor-bearing mice injected with ICG-PEG20. (A) Fluorescence images of whole mice at 3, 6, 24, 48, 72, and 168 h after administration with ICG-PEG20. White dash lines indicate tumors. (B) The time course of fluorescence intensity of tumor region in (A).

Fig. 6. Relative fluorescence intensity of tryptophan in BSA vs. sample concentration. By interaction of ICG with BSA, the fluorescence intensity of tryptophan in BSA can be changed. The binding affinity of each compound to BSA was calculated from the equation; $\log [(F_0-F)/F] = \log K_b + n \log [ICG]$. Where K_b is the binding constant, n is the number of binding sites, and F and F_0 are the fluorescence intensities of tryptophan of BSA with and without each compound, respectively. Blue, ICG-PEG20; red, ICG; green, In-DTPA-PEG20; purple, mono-amino PEG (20 kDa).

Fig. 7. SPECT/CT images of colon26 tumor-bearing mice at 24 h after the administration of ^{111}In-DTPA-PEG20. (A) CT images, (B) SPECT images, and (C) merged CT and SPECT images (A+B). The white dashed lines indicate tumor locations.

Fig. 8. PA imaging within colon26 tumor-bearing mice injected with ICG-PEG20. (A) Setting of the mouse in the instrument. The square indicates the measurement region. (B-F) PA images before and 24 h after injection of ICG-PEG20. The injected dose of ICG for ICG-PEG20 was (B) 13 nmol, (C) 26 nmol , (D) 52 nmol, and (E) 104 nmol. The dashed line circles indicate the tumor regions. (F) PA images of non-tumor regions of the back.

Fig. 9. The PA signal intensity ratios (24 h post-injection/pre-injection) plotted relative to the ICG content of injected ICG-PEG20. Data are presented as the mean ± SD.

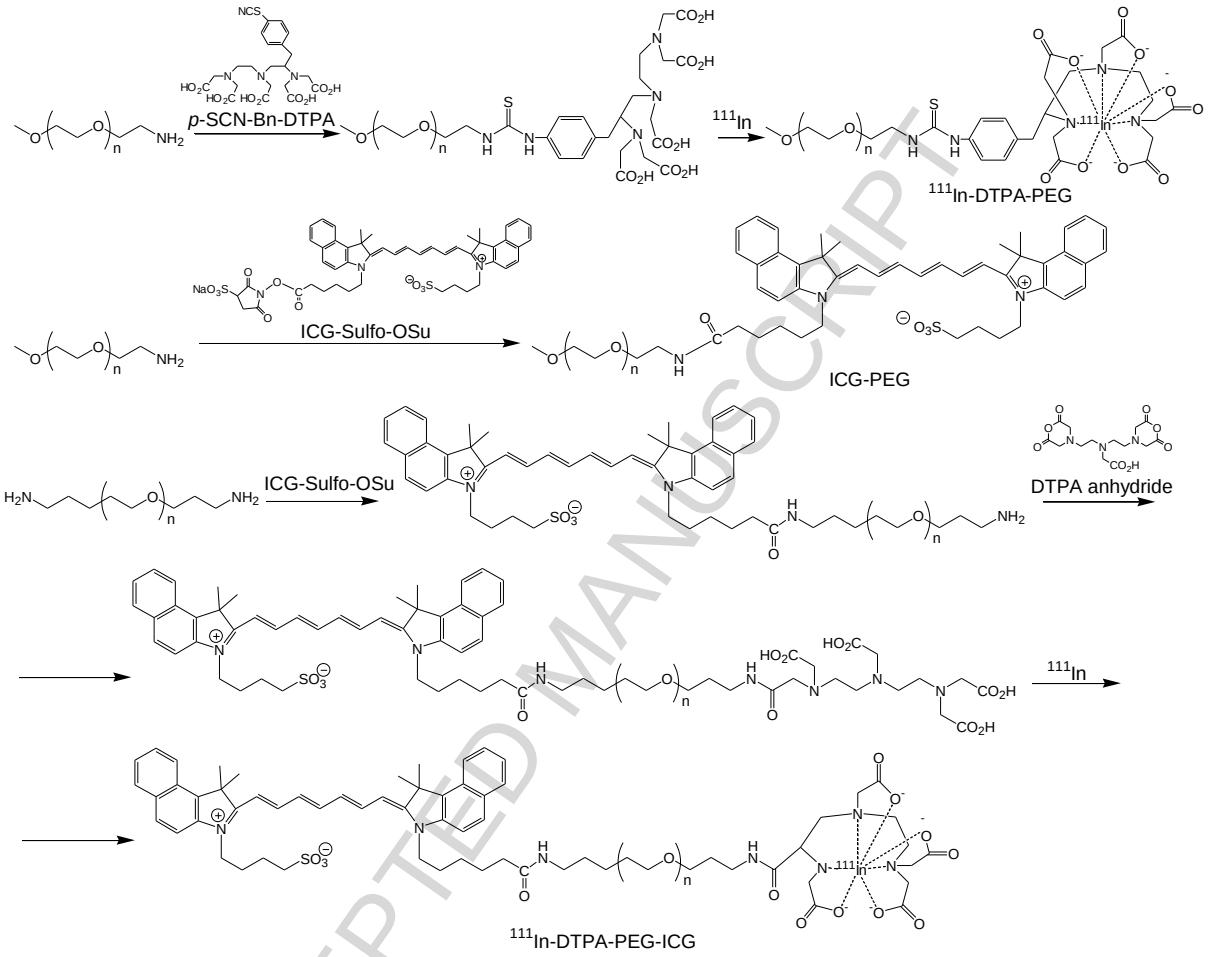

Fig. 1

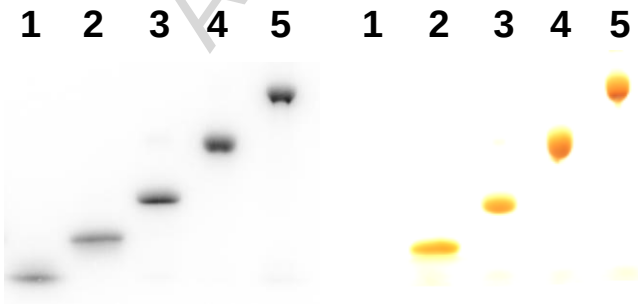

Fig. 2

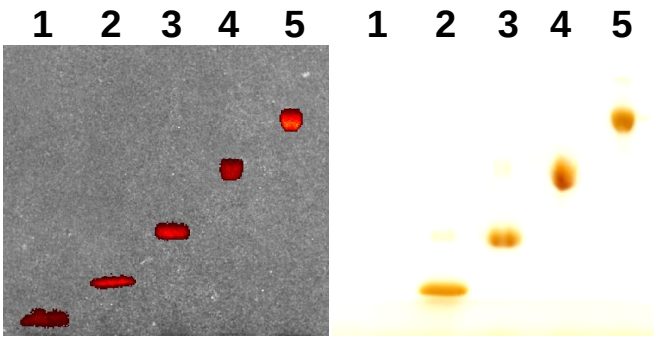

Fig. 3

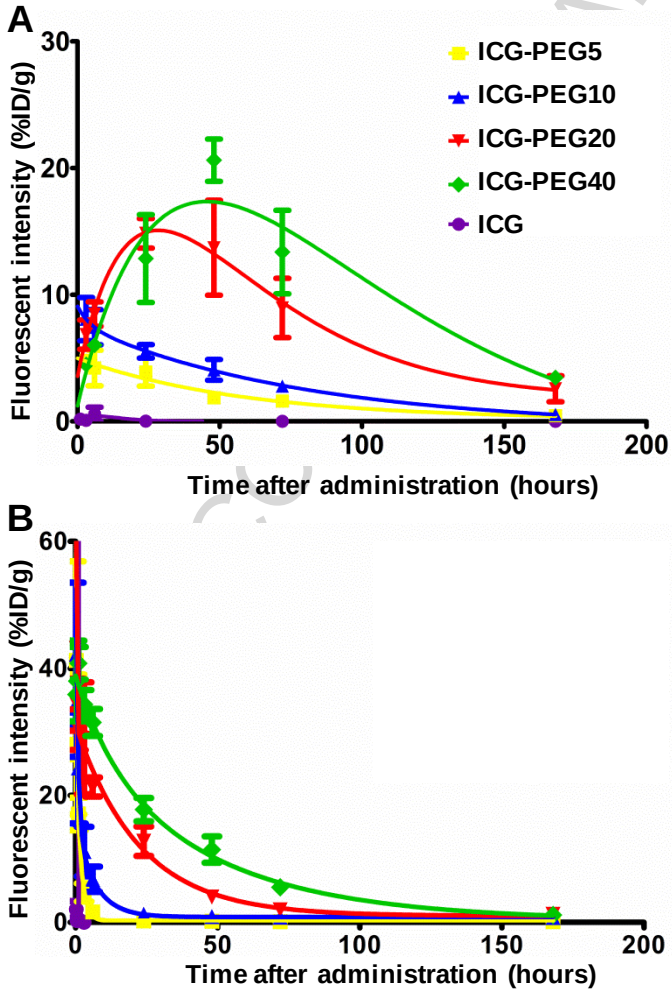

Fig. 4

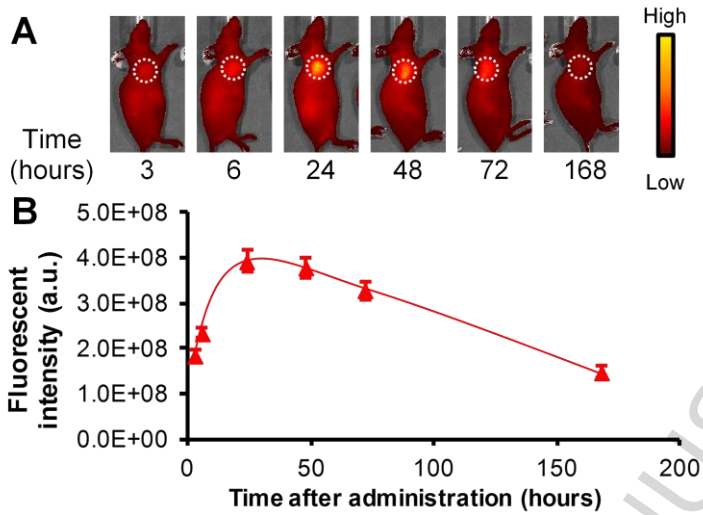

Fig. 5

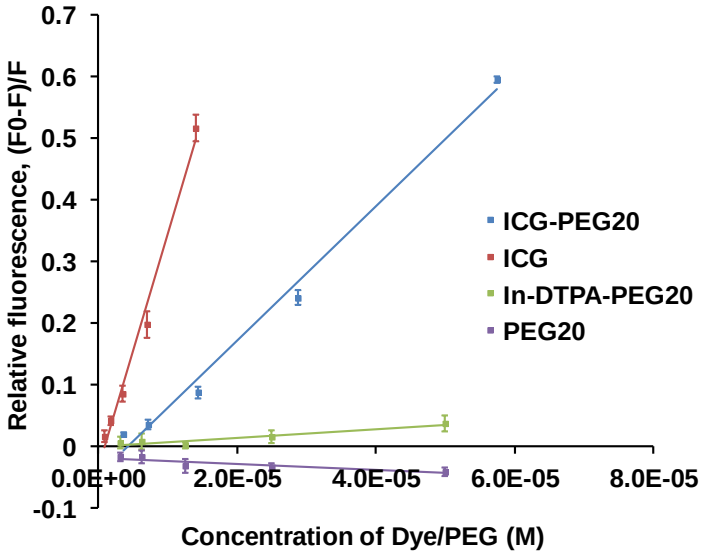

Fig. 6

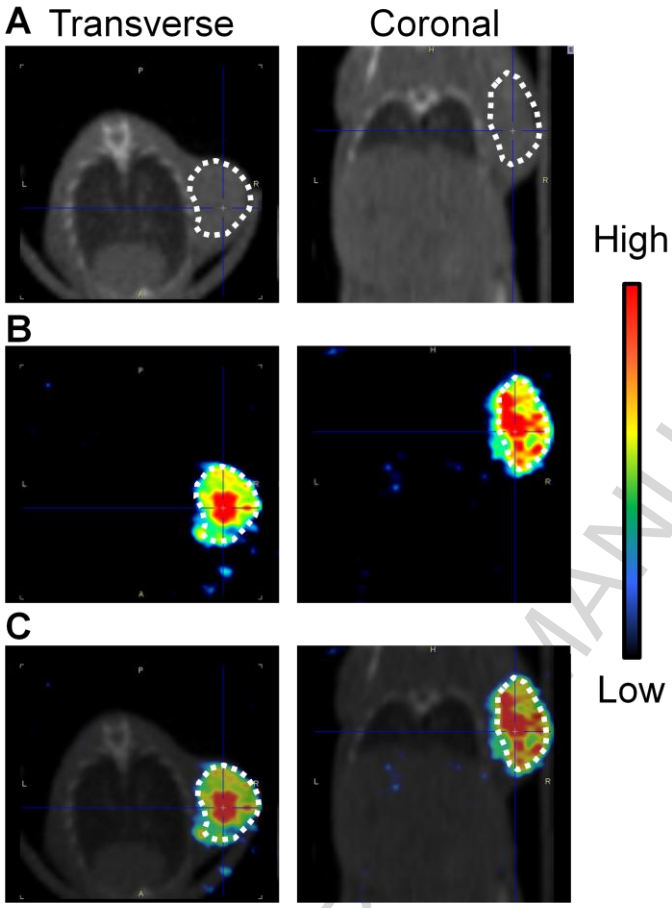

Fig. 7

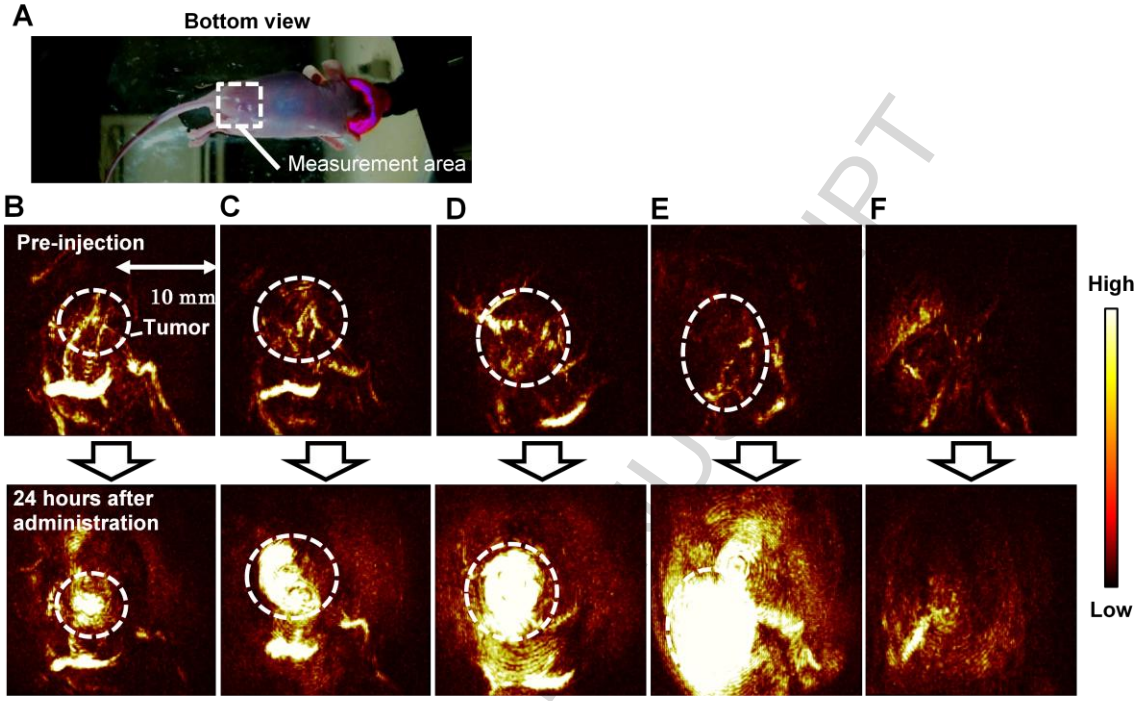

Fig. 8

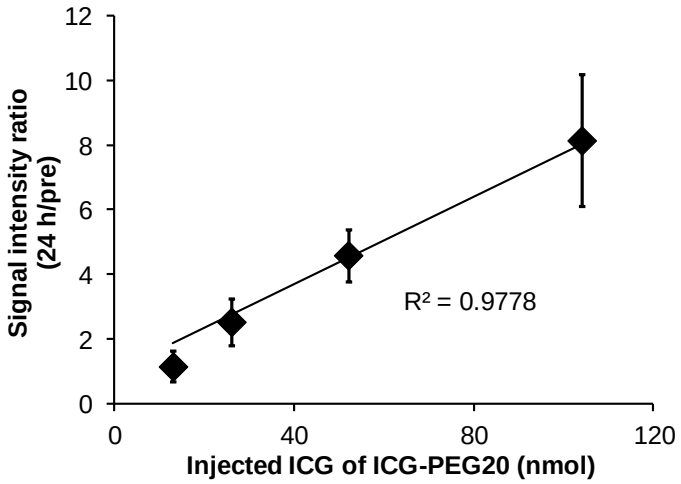

Fig. 9

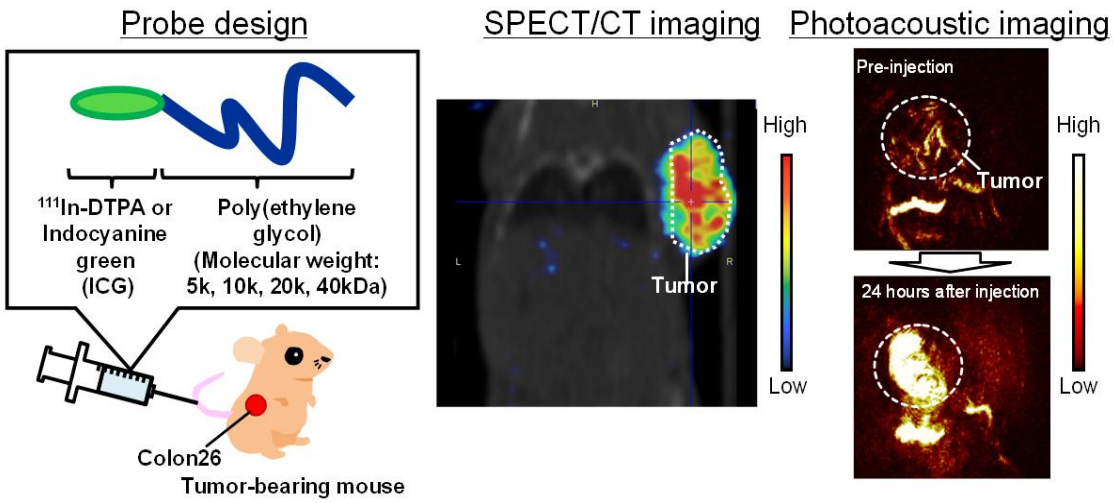

Graphical abstract